

Effects of Different Shaped Cavities and Bumps on Flow Structure and Wing Performance

A. Mahboub^{1†}, M. Bouzit¹ and A. Ghenaim²

¹ Faculty of Mechanical Engineering, Department of Mechanics, University of Sciences and Technology of Oran Mohamed Boudiaf, BP. 1505 Oran El M'Naouer, 31000 Oran, Algeria

² Icube Laboratory, Department of Mechanics, National Institute of Applied Sciences, 67084, Strasbourg, France

†Corresponding Author Email: abdelmadjid.mahboub@univ-usto.dz

(Received January 26, 2022; accepted June 18, 2022)

ABSTRACT

The stall of an aircraft is one of the most dangerous phenomena in the aviation world, resulting in a sudden loss of lift because of boundary layer separation. This work aims to delay separation and to improve wing aerodynamic performances by introducing bumps and cavities on the upper surfaces of the wing. A numerical study on the effects of both cavities and bumps on flow structures and wing aerodynamics of NACA 0012 profile is conducted. The CFX code has been used to perform calculations of steady and incompressible Reynolds Averaged Naviers-Stokes equations. The airfoil has been exposed to a free stream velocity of 5.616 m/s and chord based Reynolds number of 3.6×10^5 (chord length). A series of test on unmodified airfoil has been carried out for various turbulence models at angles of attack ranging from 0° to 15° . Then, the two-equation $k-\omega$ SST (Shear Stress Transport) has been retained for the further cases. Different configurations obtained through a modification of cavities and bumps shape, dimension, and position on the airfoil chord are investigated. Both the shapes considered are semi-spherical and semi-cylindrical, placed at two positions on the airfoil chord. The first location is in suction pick at $X/C=0.3$ and the second one is at 0.7. Results show that the application of bumps delays the boundary layer separation and increase drag coefficient. A slight enhancement in lift and drag is observed at angle of attack of 15° for the cases where the cavities are placed at 0.7 m from the leading edge. In addition, calculations show that the stability of the vortex formed inside the cavities depends strongly on their shape and the cylindrical one has better performances.

Keywords: Aerodynamics; CFD analysis; Dimple; Drag; Lift; NACA 0012; Turbulence models.

NOMENCLATURE

AOA	Angle of Attack	β^*	model constants
C	airfoil chord	μ	molecular (dynamic) viscosity
C_D	drag coefficient	μ_t	turbulent viscosity
C_L	lift coefficient	ν_t	kinetic turbulent viscosity
D	sphere and cylinder diameter	ρ	air density
e	internal energy per unit of mass	σ_k	turbulence model constant for the k equation
f	internal force per unit of mass	σ_ω	turbulence model constant for ω
F_1	blending function	τ	tensor of viscosity
k	turbulence kinetic energy per unit mass	ω	turbulent frequency
p	static pressure	β	model constants
q	heat transfer		
t	maximum relative thickness of airfoil		
V	air velocity		
(u, v, w)	Cartesian velocity components		

1. INTRODUCTION

The performance of an aircraft wing depends on its ability to produce maximum lift and less drag. Research into the effects of geometric modifications in aircraft wings, is a major asset in improving aerodynamic characteristics such as lift, drag and pitching moment on the one hand and controlling boundary layer transition and separation on the other. Theoretical studies have shown the effectiveness of trapped vortices in order to improve the aerodynamic performance of a wing profile. Vortex Cell2050, a European research project, was launched at the end of 2005 in order to study the effect of trapped vortex cavities on boundary layer separation and flow stabilisation. The idea of trapped vortex cavity is not recent. This concept has been inspired by Kasper's vortex wing who has claimed its efficiency on aerodynamics characteristics improvement and more steady flow stability. However, the experimental investigation of this configuration (Kruppa 1977) showed an unsteady vortex shedding instead. The studies of flow over airfoil with vortex trapped in a cavity carried out by Bunyakin *et al.* (1998) and Chernyshenko *et al.* (2003) have showed that for an immersed body in steady inviscid incompressible flow with two trapped vortices, the lift is non-zero with pressure favourable gradient over the entire contour body. In the flight test conducted on the aircrafts EKIP designed by L. N. Shchukin (Savitsky *et al.* 1995), wings have been thick with four cavities on the downstream of the upper surface and a central body inside the cell to form a ring that makes flow more stable. A computational analysis of cavity effects with square and triangular shape has been performed by (Booma and Shah 2016). The results have showed an increase in lift coefficient with downstream delaying stall angle. Sowmyashree *et al.* (2020) have showed the lift enhancement and drag decrease provided by the application of dimple (cavity) on NACA 2412 at 80mm from the leading edge (which is a 0.8 chord length) in the lower surface of airfoil. They have also reported that the inward cavity is more efficient than the outward one. Cavities can be considered as deep or shallow depending on the ratio of cavity depth to cavity opening. The aerodynamics characteristics are highly affected by the instability and the oscillation of shear layer above the cavity by interfering with Van Kerman shedding. Several studies have been performed on cavity flow characteristics prediction with application of Euler equations resolutions and others methods based on Navier-Stokes equations resolution. Bres and Colonius (2008) have presented a result of tridimensional instability of compressible flow, over open cavity with direct numerical simulations, for various cavity aspect ratios. They have observed the existence of oscillating span wise structure inside the cavity. A numerical analysis of flow around circular cylinder with two vortices cells has been carried out by Isaev *et al.* (2014). A fan draws air from the two cavities, via slots and discharges it through a central channel. At the outlet the low-

pressure air, leads to a rearrangement of large flow structures, around the cylinder with a suppression of Karman Vortex Street, which stabilises the wake, resulting in a reduction of the frontal drag. Fatehi *et al.* (2018) have presented aerodynamic characteristics of wind turbine blade with cavity shape optimisation, using the genetic algorithm. Then results have been compared with experimental ones at same configuration of max performance, provided by numerical method. A significant increment has been obtained in lift to drag ration 31% at AOA=14° and 57% at AOA=20°. The trapped vortex cavity (TVC) as passive and active flow control has been performed by Gregorio and Fraioli (2008). They have reported that a passive TVC cannot control the boundary layer separation. A decrease in aerodynamic characteristics, due to a vortex shedding compared to clean airfoil, has been noticed. However, full reattachment has been obtained by active TVC. Narayana *et al.* (2018) have investigated the effect of dimple on the aerodynamic wing performances. Test has included inward and outward dimples with different aspect ratios, and placed at two different positions on NACA 4415. It has been shown that better performances are obtained with inward dimple at 80% of chord length with 0.2 aspect ratio of dimple. However, studies carried on NACA 0018 (Srivastav 2012) have shown that outward dimple, produces less drag for positive angle of attack. Prasath and Irish Angelin (2017) have performed experimental analysis on dimple effect on aerodynamic characteristics of NACA 0018 wing airfoil. Thirteen dimples are created along the span wise direction, at 40% from the leading edge, on both upper and lower surface. The results have showed that dimpled airfoil produces less drag and increases lift coefficient with a delay in flow separation. Therefore, stall occurs later than clean airfoil.

This work shows CFD analysis of the flow behaviour and performances of a modified wing, by introducing cavity and bump on the upper surface.

Several configurations are tested by changing three parameters, the shape, the size of the cavities (bumps) and the position from the leading edge of the wing. The study consists in defining the aerodynamic characteristics of the different configurations such as the lift coefficient, the drag coefficient and the glide ratio.

2. COMPUTATIONAL DETAILS AND METHODOLOGY

2.1 Governing equations of fluid movement

Air movement is described by the set of Navier-Stokes equations, of continuity, momentum and energy (Katz and Polotkin 1991; Roy 1988). These partial derivative equations are shown as follows, in simplified form.

Continuity equation:

$$\frac{\partial \rho}{\partial t} + \nabla \cdot (\rho \vec{V}) = 0 \quad (1)$$

Momentum equation:

$$\frac{\partial}{\partial t} (\rho \vec{V}) + \nabla \cdot (\rho \vec{V} \vec{V}) = -\nabla p + \rho \vec{f} + \nabla \cdot \tau \quad (2)$$

Energy equation:

$$\rho \frac{D}{Dt} \left(e + \frac{1}{2} V^2 \right) = \nabla \cdot (p \cdot \vec{V}) - \nabla \cdot \vec{q} + \rho \vec{f} \cdot \vec{V} \quad (3)$$

2.2 Airfoil and Domain Configuration

The chosen profile is NACA 0012 geometry, which is determined by the following expression (Moran 1984):

$$\pm y = \frac{t}{0.2} \left(0.2969 \sqrt{x} - 0.1260x - 0.3537x^2 + 0.2843x^3 - 0.1015x^4 \right) \quad (4)$$

The formatted airfoil data points are imported to ICEM CFD. The chord length of the airfoil is $C=1\text{m}$ with small span length of $0.2C$. The computational domain is $20C$ in all the directions from the leading edge, as shown in previous studies (Sørensen 2009; Tang 2008) (Fig. 1). The wing modification is obtained by introducing cavity and bumps on the upper surfaces of the airfoil. Both spherical and cylindrical shapes are considered (Fig.2). The simulation is done for various diameter of cavity and bump, located at two positions from the leading edge along the chord (Table 1).

2.3 Meshing

A structured hexahedral mesh using ICEM CFD is adopted by the creation of multiple blocks associated to the geometry (Fig. 3). A test of mesh size from the coarsest to the finest has been carried out in order to ensure that the results no longer depend on the number of meshes. The tests have been carried out with 1.9 million, 2.4 million, 3.5 million, 5 million and finally 5.5 million meshes. It has been found out that, from 5 million meshes

onwards, the results have remained unchanged (Fig. 5). Hence, this type of mesh use has been adopted. The detailed distribution of nodes number is as follows: 120 nodes along the upper surface of the wing and 120 along the lower surface; 185 knots in vertical direction of the wing wall; 130 knots from trailing edge to the OUTLET. In order to scale a Y^+ of less than one, the first mesh size in the near wall is 10^{-5} C. The numerical results are strongly affected by the quality of the mesh, in particular, the contributions of the error sources due to the discretisation of the transient/storage, diffusion, source and Rhie-Chow redistribution terms increase with a disordered mesh. Therefore, several criteria have been taken into account in the design of the mesh, such as; an orthogonality greater than 72° , a volume ratio of two consecutive meshes less than 2, and a maximum aspect ratio of 1.9×10^4 which is

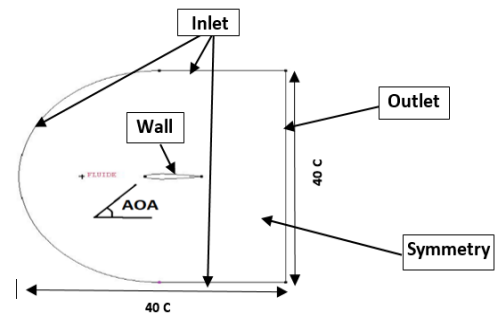


Fig. 1. Airfoil and domain configuration

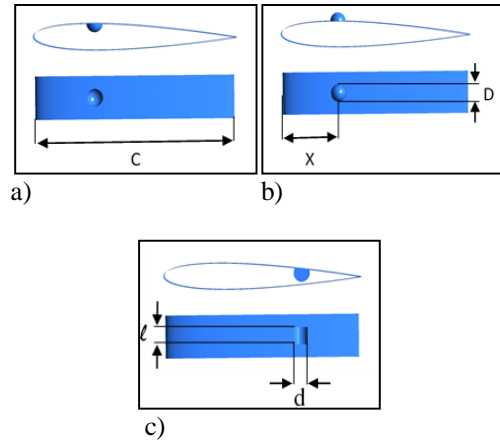


Fig. 2. Modified airfoil, a) Spherical cavity, b) Spherical bump, c) Cylindrical cavity.

Table 1 Characteristics of the investigated Cases

Case	Shape	X/C	D/C	l/C	d/C
A	Spherical cavity	0.3	0.04	-	-
B	Spherical cavity	0.3	0.06	-	-
C	Spherical cavity	0.3	0.08	-	-
D	Spherical bump	0.3	0.04	-	-
E	Spherical bump	0.3	0.06	-	-
F	Spherical bump	0.3	0.08	-	-
G	Spherical cavity	0.7	0.08	-	-
H	Cylindrical cavity	0.7	0.08	0.08	0.08
I	Cylindrical cavity	0.7	0.08	0.08	0.07

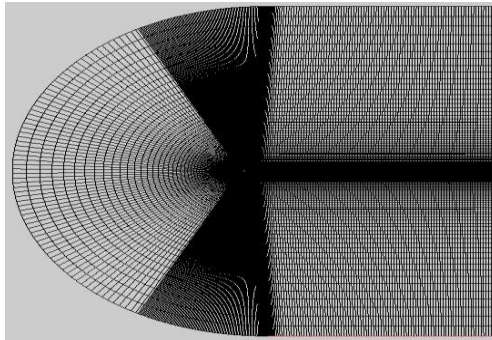


Fig. 3. C-structured domain meshing.

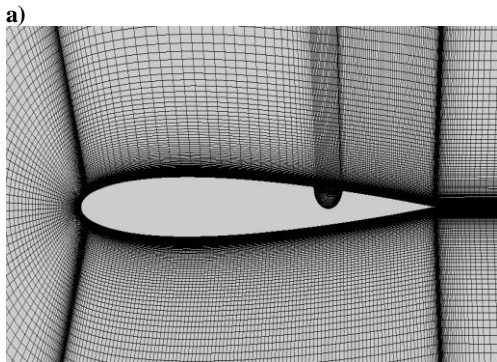
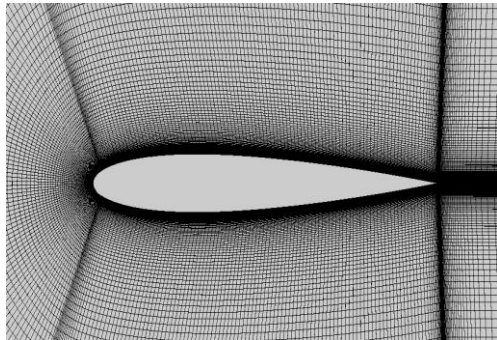


Fig. 4. Near airfoil refinement mesh, a) Clean airfoil, b) Airfoil with cavity

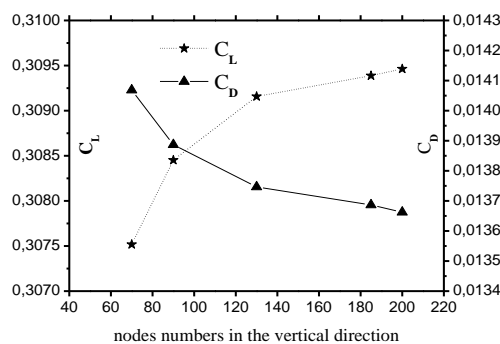


Fig. 5. Results of the grids independence study.

an acceptable value in double precision. In order to reduce the computation time, the number of meshes has been reduced by adopting a very fine mesh, close to the walls and increasingly coarse mesh far from the wing walls. In order to do this, the GEOMETRIC1 and 2 law has been used with a ratio of 1.14 (Figs. 4 (a); (b)).

2.4 Boundary Conditions

Mathematical models in science and technology are very often presented as systems of differential equations that relate unknown functions to their partial derivatives. Initial and boundary conditions are usually required to complete the model (Fig.1). In this work, the boundary conditions adopted are as follows: Air speed of 5.616 m/s at the domain inlet, which corresponds to a Reynolds number of $3.6 \cdot 10^5$, based on the chord length of the airfoil; an exit pressure of zero relative to a reference pressure of one atm. The two sides of the domain are considered symmetrical. Finally, the wing surface is subjected to the wall condition with friction. A new coordinate system is created for each angle of attack, in order to avoid the design of a new geometry and a new mesh for each case studied.

2.5 Numerical Details

The method of resolution on which the CFX calculation code is based is known as the finite volume method. At first tests are conducted for clean airfoil using various turbulent models at AOA ranging from 0° to 15° (Figs. 7, 8). Then $k-\omega$ SST is retained for the further cases, as it gives very accurate predictions of the occurrence and amount of flow separation under negative pressure gradients. The following conditions are set for the calculation. Table 2 represents the test of residual target effect on results, so the value of 10^{-6} is chosen. The advection scheme is set to High-resolution, used for continuity and momentum equations, in order to reduce source of solution error and get accurate result. It uses a special nonlinear recipe for β at each node, based on the boundedness principles used by Barth and Jespersen (1989). An auto timescale with conservative length scale is used to progress the simulation. The time scale factor has been set to 0.1 at high angle of attack. This leads to a decrease RMS oscillating period and to linear convergence.

$k-\omega$ SST (Shear Stress Transport) equations are as follows (Eleni *et al.* 2012):

$$\frac{D\rho k}{Dt} = \tau_{ij} \frac{\partial u_i}{\partial x_j} + \beta^* \rho \omega k + \frac{\partial}{\partial x_j} [(\mu + \sigma_k \mu_t) \frac{\partial k}{\partial x_j}] \quad (5)$$

$$\frac{D\rho \omega}{Dt} = \frac{\gamma}{\nu_t} \tau_{ij} \frac{\partial u_i}{\partial x_j} + \frac{\partial}{\partial x_j} [(\mu + \sigma_\omega \mu_t) \frac{\partial \omega}{\partial x_j}] + 2\rho(1 - F_1)\sigma_\omega \frac{1}{\omega} \frac{\partial k}{\partial x_j} \frac{\partial \omega}{\partial x_j} - \beta\rho\omega^2 \quad (6)$$

Table 2 Test of Residual Target Effect on Result

RMS	ΔC_L	ΔC_D
$10^{-5} \rightarrow 10^{-6}$	$5.241 \cdot 10^{-3}$	$1.996 \cdot 10^{-4}$
$10^{-6} \rightarrow 10^{-7}$	$3.33 \cdot 10^{-4}$	$1.15 \cdot 10^{-5}$
$10^{-7} \rightarrow 10^{-8}$	$3.3 \cdot 10^{-5}$	$2 \cdot 10^{-6}$

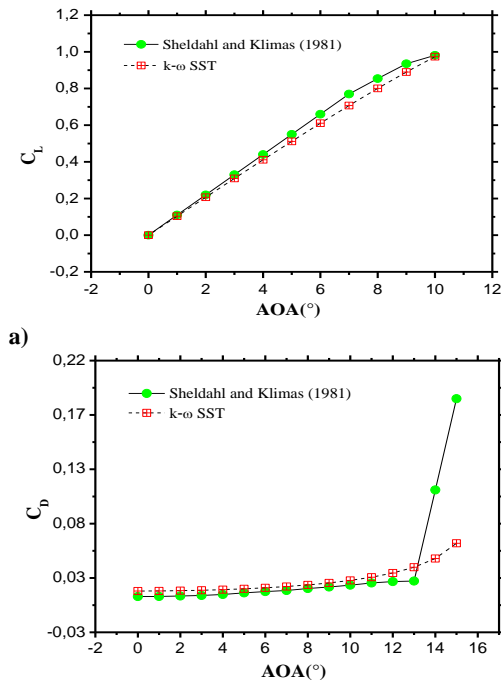


Fig. 6. Validation of numerical results, (a) Lift coefficient versus AOA, (b) Drag coefficient versus AOA.

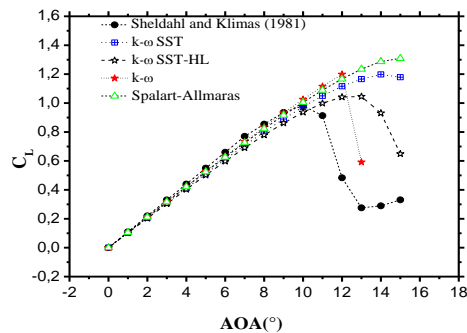


Fig. 7. Influence of turbulence model on lift coefficient.

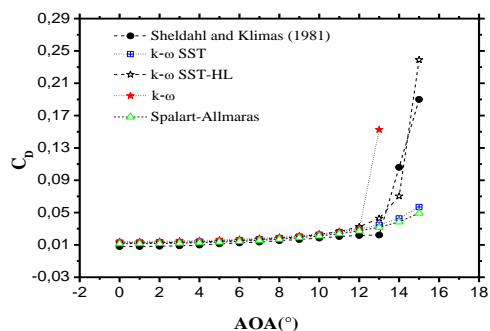


Fig. 8. Influence of turbulent model on drag coefficient

3. RESULTS AND DISCUSSION

The best way to define the aerodynamic performance of an aircraft wing is to plot its characteristic curves such as the lift and drag coefficients as a function of the angle of attack, the

polar, the glide and finally its pressure coefficient which defines the pressure distribution around the wing.

The numerical method is validated by comparing the CFD results of lift and drag coefficients (Fig.6 (a),(b)), to experimental data provided by [Sheldahl and Klimas \(1981\)](#). The figure shows that the predicted results are in good agreement with experiments except at higher angle of attack where discrepancy occurs due to the increase in the adverse pressure gradient, and the unsteadiness of the flow before the stall.

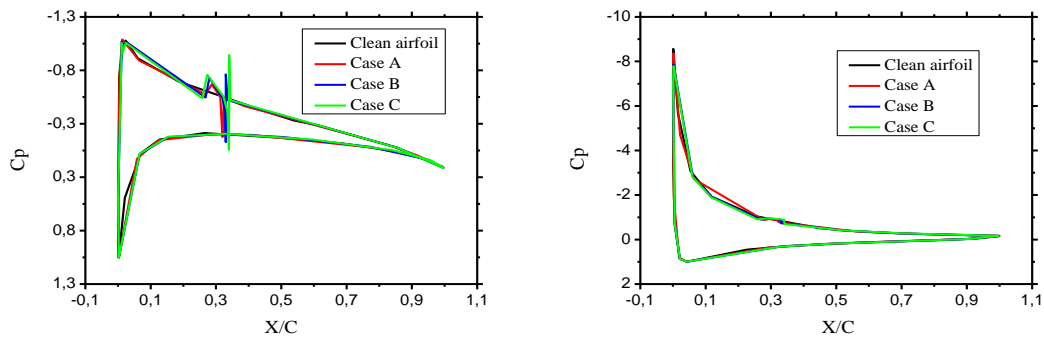
As the angle of attack increases, the lift coefficient will increase. It can be seen that this increase is linear and from a certain angle, the lift point is too far forward and the lift coefficient reaches its maximum and then undergoes a sudden drop (Fig. 7). This phenomenon is called the stall. It can be seen that at low angles of attack the drag coefficient is low and it changes only slightly with small changes of angle of attack. However, as the angle of attack increases, the drag coefficient increases and at the upper end of angle of attack range, even small changes in angle of attack produce a significant increase in drag. At the stall, a large increase in drag occurs (Fig.8). The PIV measurements carried out by ([Avelar *et al.* 2006](#)) show that the stall angle of NACA 0012 is around 15.5° for Reynolds number of 2.5×10^5 and around 16.5° for Reynolds number of 4.0×10^5 . It has been shown that for high angles of attack, the turbulence models used by computational codes are inaccurate ([Eleni *et al.* 2012](#)); and that 15° is the limit beyond which numerical errors become increasingly important and instabilities appear. As a result, RANSE models fail to capture boundary layer separation, turbulence and eddies ([Janardhanan and Thaliyakkattil 2015](#)).

Compared to the experimental results obtained by ([Sheldahl and Klimas 1981](#)), both the turbulence models, the k- ω SST and the Spalart-Allmaras, overestimate the maximum lift coefficient as well as the stall angle, which is estimated at 14 and 15 degrees respectively (Figs. 7, 8). Physically, this translates into the fact that both models predict a weak and late boundary layer separation, as observed in the experimental results. By using the k- ω model, the stall angle (12°) is estimated more accurately than the previous models. However, the k- ω SST-HL model, which is a modified version of the k- ω SST model, allows the stall angle, estimated at 12°, and the maximum lift coefficient to be predicted more accurately than the previous models, by introducing a tuning parameter (CHL coefficient), which allows the k- ω SST model to be adjusted for such applications. The default value of this parameter is 0.9. In order to return to the k- ω SST model, it is sufficient to impose a value of one on this parameter. It is worth noting that all the other available eddy-viscosity models lead to even stronger deviations from experimental data compared to the k- ω SST model and so they do not offer an alternative to the k- ω SST-HL

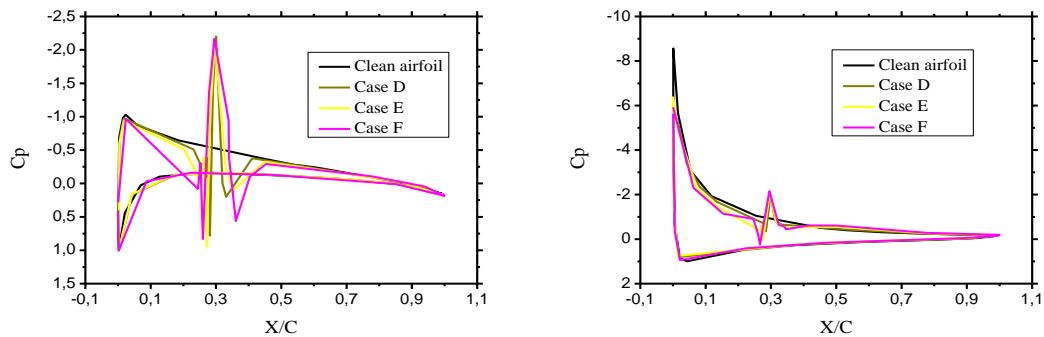
modification. It should be noted that the $k-\omega$ SST model gives results that are more accurate at small angle of attacks. This is the reason why $k-\omega$ SST has been adopted for all further cases.

Figures 9, 10 and 11 show the static pressure distribution around the wing, for the models with and without modification, for two angles of attack of 3° (a), 15° (b). The results show that as the angle of attack increases, the pressure difference between the lower and upper surface increases, and consequently the lift force, which is proportional to the area between these two distributions increases. However, above a certain value of the angle of

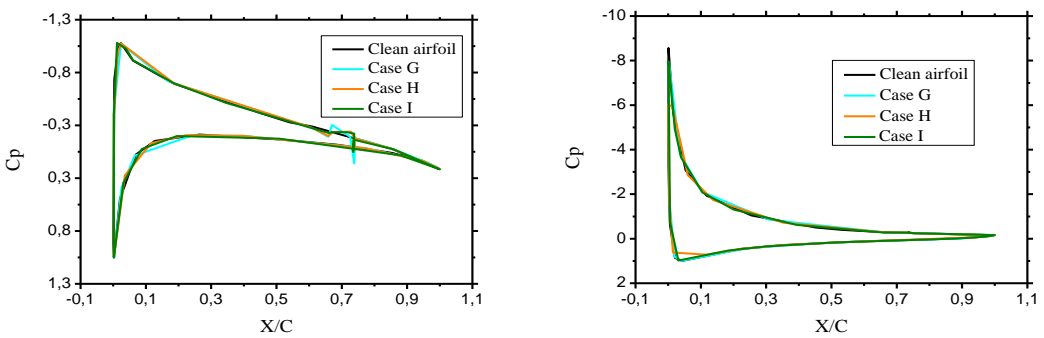
attack, the wing stalls due to the separation of the boundary layer. It is also observed that there is a negative pressure peak near the leading edge, resulting in a strong acceleration of the airflow on the upper surface. Therefore, different flow behaviour is observed for the various configurations. Results show that pressure is more affected by bumps (case D, E, F) than cavities. On the other hand, it can be noticed that modifications made at $X/C=0.3$ have more significant influence than the ones made at $X/C=0.7$. It is also noticeable that as the angle of attack increases, there is less and less effect on the pressure distribution around the wing, for all the configurations.



a) b)
Fig. 9. Pressure coefficient distribution on airfoil surface at $Z=0.1m$ for case A, B, C, compared to clean airfoil, a) $AOA=3^\circ$, b) $AOA=15^\circ$.



a) b)
Fig. 10. Pressure coefficient distribution on airfoil surface at $Z=0.1m$ for case D, E, F, compared to clean airfoil, a) $AOA=3^\circ$, b) $AOA=15^\circ$.



a) b)
Fig. 11. Pressure coefficient distribution on airfoil surface at $Z=0.1m$ for case G, H, I, compared to clean airfoil, a) $AOA=3^\circ$, b) $AOA=15^\circ$.

The u velocity inside the cavity and near airfoil wall is plotted (Figs. 12, 13, 14). In these graphs, negative values of the velocity u , which corresponds to the formation of vortices inside the cavity (cases A, B, C, G, H, I), can be seen. It can also be seen that the maximum speed is obtained for the cases where the wing is provided with bump (case D, E, F). This can be explained by the narrowing of the frontal section of the flow on the one hand; and by the turbulent and anisotropic flow produced by the application of cavity, which acts as an aerodynamic band fraying the flow. This last is well evidenced by the graph expressing the velocity w in the span wise direction, which is different from zero (Fig. 15). However, the intensity of the transverse flow inside the cavities depends strongly on their shape as well as their depth. It is clear that

the cylindrical shape with a low ratio (d/D) is recommended for the creation of more stable vortices with a favourable direction of rotation to create less resistance to the flow around the wing.

The best way to know the performance of an aircraft wing is to determine its aerodynamic characteristics, such as lift and drag coefficients and especially C_L to C_D ratio (Fig. 16). It can be seen clearly that at 3° angle of attack (Fig. 16 (a)), the configuration (F) has the highest lift coefficient, but the drag coefficient is also the highest. In terms of C_L to C_D ratio it is not the best possible configuration. By comparing the cases (C) and (G), which are two identical cavities, except for their respective positions, the case (G) gives better results. Therefore, it can be noticed easily that the

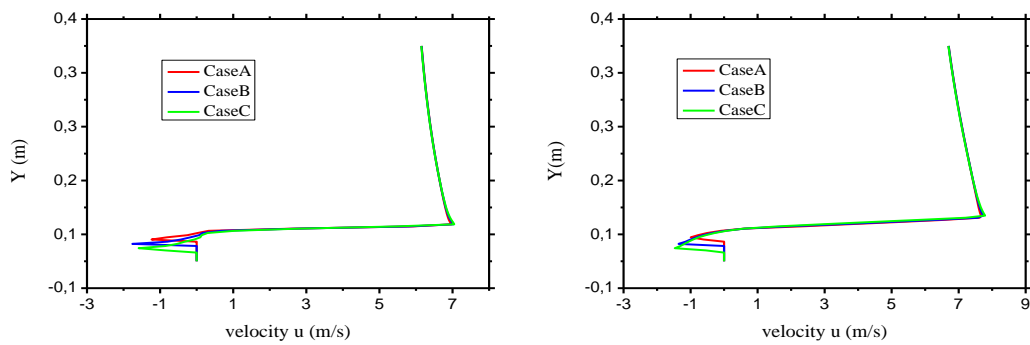


Fig. 12. Velocity u for cases A, B, C, at line $X/C=0.3$ and $Z=0.1m$ a cross cavity center, a) $AOA=3^\circ$, b) $AOA=15^\circ$.

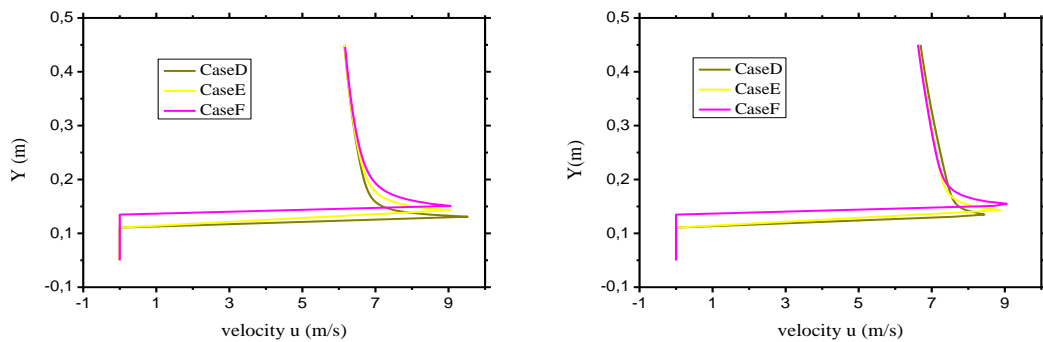


Fig. 13. Velocity u for cases D, E, F, at line $X/C=0.3$ and $Z=0.1m$ a cross dimple center, a) $AOA=3^\circ$, b) $AOA=15^\circ$.

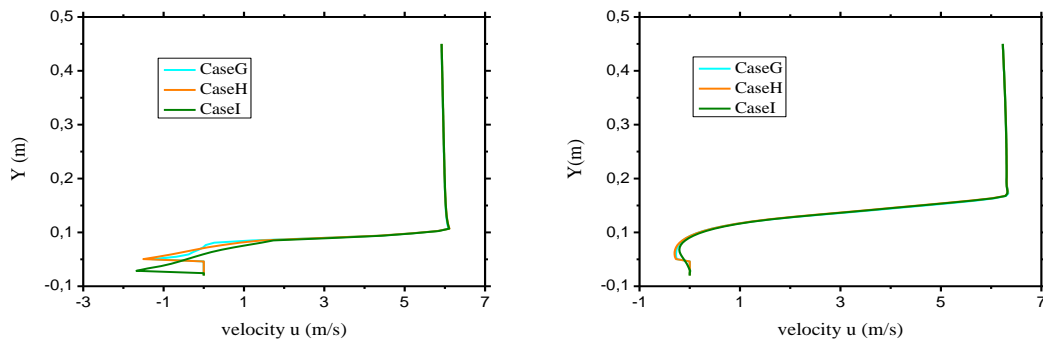


Fig. 14. Velocity u for cases G, H, I, at line $X/C=0.7$ and $Z=0.1m$ a cross cavity center, a) $AOA=3^\circ$, b) $AOA=15^\circ$.

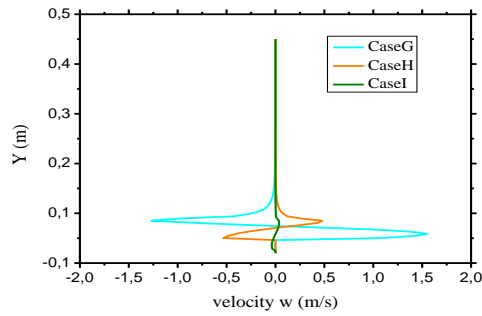


Fig. 15. Velocity w for case G, H, I, at line $X/C = 0.7$ and $Z=0.1m$ at cross dimple center, $AOA=3^\circ$.

unmodified profile has better performance. However, at 15° , a slight enhancement is observed (Fig.16 (d)); configuration (G) has the highest lift coefficient and the lowest drag coefficient. Similarly, configuration (H) and (I) perform better than the unmodified wing but it is still a very small improvement in performance.

The static pressure contours at 3° and 15° angle of attack are shown in Figures 17, 18, for the different configurations. It is clear that the lower surface of the wing is over pressurised, while there is a negative pressure on the upper surface. This is directly reflected in the creation of the lift force perpendicular to the relative wind. On the other hand, the creation of the drag force is a consequence of the pressure distribution between the upstream and the downstream sides of the wing as well as the viscosity forces exerted on its walls. The pressure contours show that the pressure at the leading edge, which is an impact zone, where the pressure is maximum, is clearly higher than the one

at the trailing edge.

The flow velocity contour and streamlines around airfoil at angles of attack of 3° , 15° are presented in Fig. 19, 20, 21 and 22. It can be noticed that the stagnation point at the trailing edge advances slowly towards the leading edge for small angles of attack, but as soon as critical angles are approached, a sudden shift towards the leading edge is noticed, as demonstrated by previous studies (Eleni *et al.* 2012).

As expected, based on the distribution of static pressures around the wing, and the Bernoulli equations that highlight the relationship between velocity and static pressure, the results have showed that the airflow at the upper surface undergoes an acceleration that is greater as the angle of attack increases. It is also noted that the suction peak at the point of maximum velocity moves towards the leading edge as the angle of attack increases. As a result, and with the separation of the boundary layer at the trailing edge, the point of application of the aerodynamic resultant (centre of pressure) also moves towards the leading edge, until the wing stalls completely. A reattachment of separated boundary layer is observed in the cases (D, E, F), as shown in Fig. 20, due to bump application.

It is also noticed that the vortices at 3° are formed entirely inside the cavities (Fig. 21) contrary to the ones at 15° angle of attack, a part of which is outside (Fig. 22). This can be explained by a periodic shedding of the vortex.

Figures 23, 24 show the static pressure over the whole wing surface and 3D streamline of the thin boundary close wing.

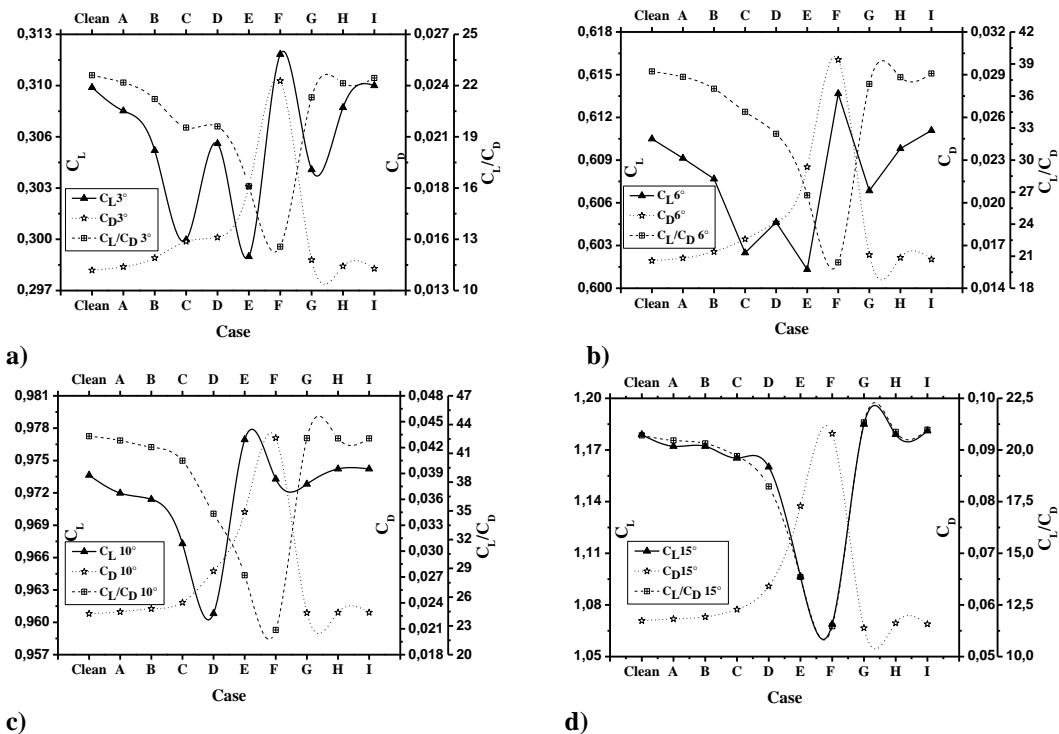


Fig. 16. Airfoil aerodynamic characteristics with and without modification for different configuration, a) $AOA=3^\circ$, b) $AOA=6^\circ$, c) $AOA=10^\circ$, d) $AOA=15^\circ$

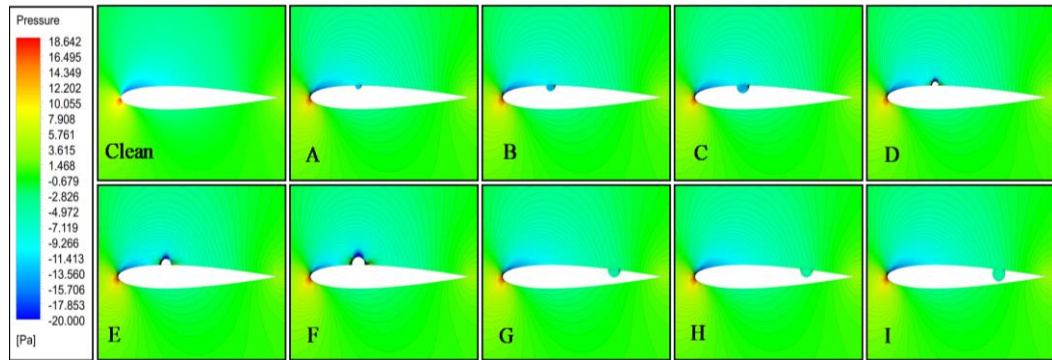


Fig. 17. Pressure contours plan $Z=0.1m$; $AOA=3^\circ$.

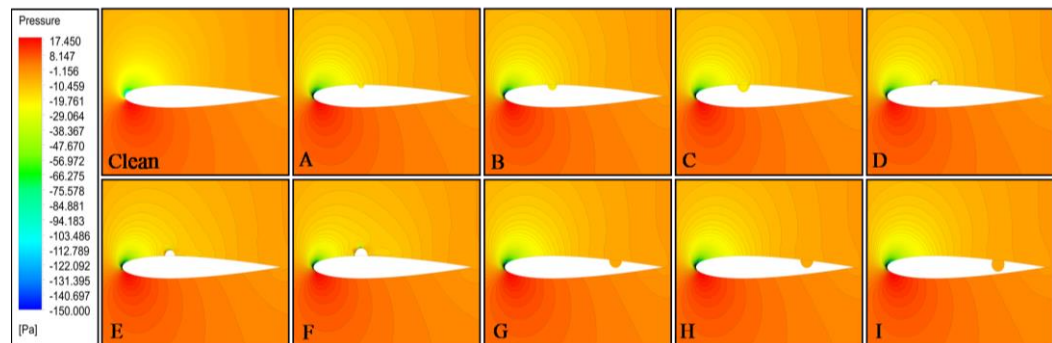


Fig. 18. Pressure contours plan $Z=0.1m$; $AOA=15^\circ$.

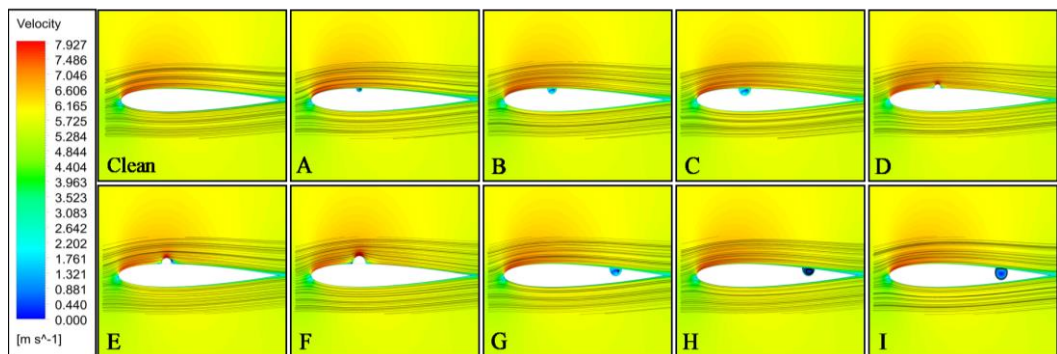


Fig. 19. Velocity contours plan $Z=0.1m$ with streamline; $AOA=3^\circ$.

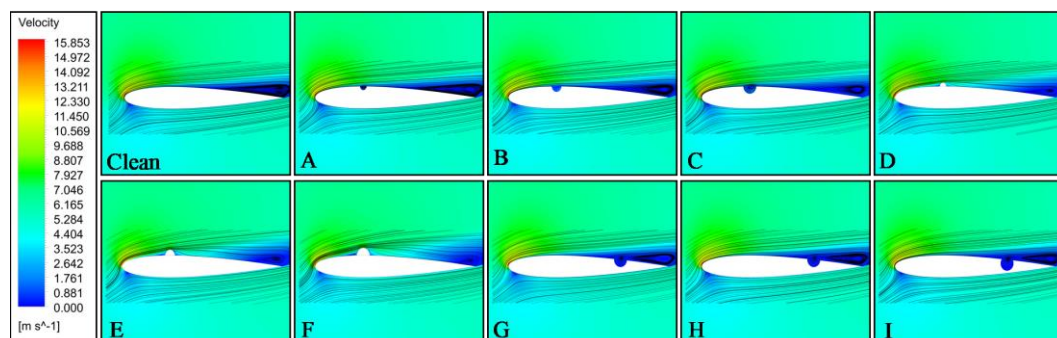


Fig. 20. Velocity contours plan $Z=0.1m$ with streamline; $AOA=15^\circ$.

4. CONCLUSION

The results obtained show that the numerical

models used in the study of the flow around a wing with NACA 0012 airfoil, are reliable up to a certain limit where the adverse pressure gradients become

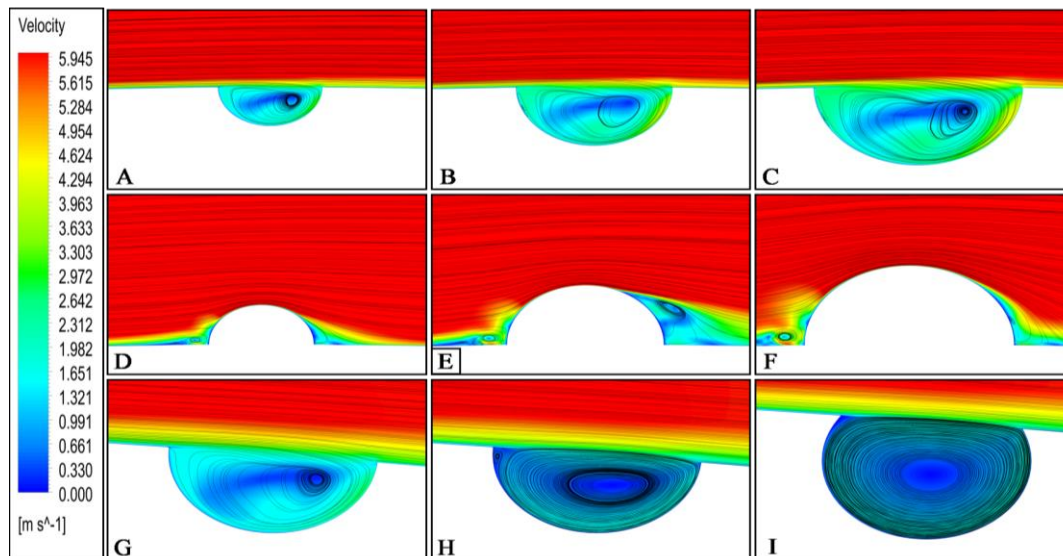


Fig. 21. Velocity contours with streamline cavity at $X/C=0.3$ plan $Z=0.1m$; $AOA=3^\circ$

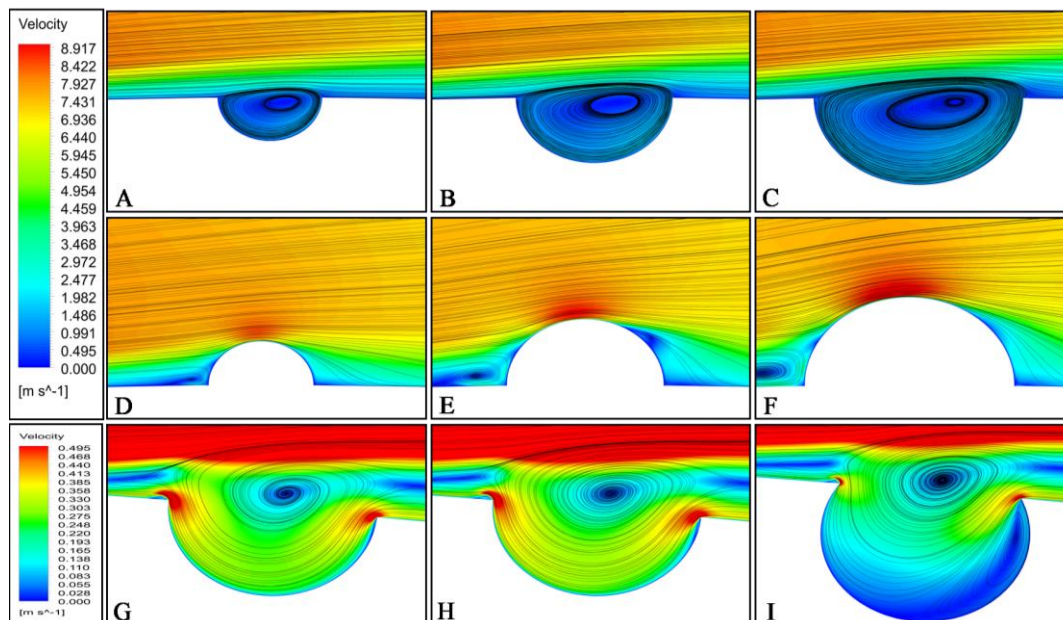


Fig. 22. Velocity contours with streamline cavity at $X/C=0.3$ plan $Z=0.1m$; $AOA=15^\circ$

increasingly large, which makes the modelling of the detached boundary layer very difficult. The prediction of the lift and drag coefficients is in good agreement with the results obtained by [Sheldahl and Klimas \(1981\)](#), except in the prediction of the stall angle and the maximum lift coefficient which are overestimated by all the turbulence models used.

The results obtained have shown the effectiveness of bumps in delaying boundary layer separation, but their use increases significantly the drag forces.

A reattachment of the separated boundary layer is observed in the cases (D, E, F), due to bump application.

The use of cylindrical cavities is desirable as it

reduces the transverse component of the velocity and provides greater stability of the vortices. However, the effect of the cavities on aerodynamic performances is minimal. Therefore, a slight enhancement at 15° for cavities located at $X/C=0.7$ is noticed.

It can be concluded, that the improvement of aerodynamic performances, by vortices trapped inside cavities can be achieved by feeding these vortices with an external source of energy. This favours a smooth flow, which reduces the friction forces, and consequently the total drag of the wing and increase of the lift by the acceleration of the air stream on the upper surface.

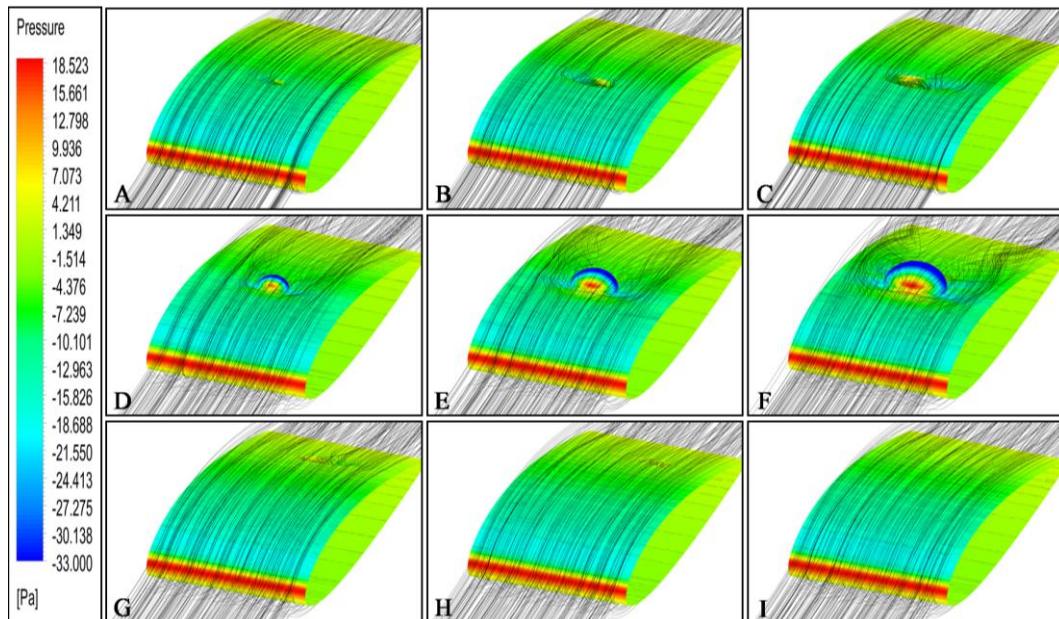


Fig. 23. Pressure over wing's surfaces with 3D streamlines; AOA= 3°

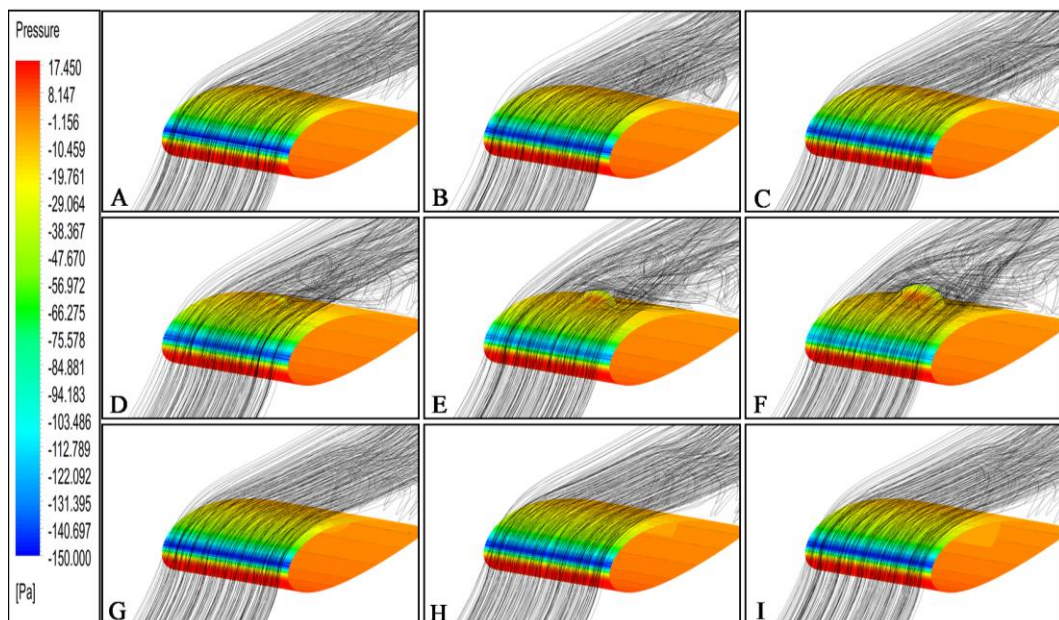


Fig. 24. Pressure over wing's surfaces with 3D streamlines; AOA=15°

References

- Avelar, A. C., L. A. Santos, O. A. F. Mello and J. Pagani (2006). A PIV Study of the Flow around a NACA 0012 Airfoil in a Subsonic Wind Tunnel. *25th AIAA Aerodynamic Measurement Technology and Ground Testing Conference*, San Francisco, California, 3143.
- Barth, T. J. and D. C. Jespersen (1989). The Design and Application of Upwind Schemes on Unstructured Meshes. *27th Aerospace Sciences Meeting*, Reno, Nevada, 0366.
- Booma, P. and D. A. Shah (2016). Computational Analysis of Cavity Effect Over Aircraft Wing. *International Journal of Mechanical, Aerospace, Industrial, Mechatronic and Manufacturing Engineering* 10(4), 774-777.
- Bres, G. and T. Colonius (2008). Three-Dimensional Instabilities in Compressible Flow over Open Cavities. *Journal of Fluid Mechanics* 599(Mar.), 309-339.
- Bunyakina, A. V., S. I. Chernyshenko and G. Y. Stepanov (1998). High-Reynolds-Number Batchelor-Model Asymptotics of a Flow Past an Aerofoil with a Vortex Trapped in a Cavity. *Journal of Fluid Mechanics* 358(1), 283-297.

- Chernyshenko, S. I., B. Galletti, A. Iollo and L. Zannetti (2003). Trapped Vortices and a Favourable Pressure Gradient. *Journal of Fluid Mechanics* 482(May.), 235-255.
- Eleni, D. C., T. I. Athanasios and M. P. Dionissios (2012). Evaluation of the Turbulence Models for the Simulation of the Flow over a National Advisory Committee for Aeronautics (NACA) 0012 Airfoil. *Journal of Mechanical Engineering Research* 4(3),100-111.
- Fatehi, M., M. Nili-Ahmadabadi, O. Nematollahi, A. Minaean and K. C. Kim (2018). Aerodynamic Performance Improvement of Wind Turbine Blade by Cavity Shape Optimization. *Renewable Energy* 132 (Mar.), 773-785
- Gregorio, F. D. and G. Fraioli (2008). Flow Control on a High Thickness Airfoil by a Trapped Vortex Cavity. *14th Int Symp on Applications of Laser Techniques to Fluid Mechanics*, Lisbon, Portugal, 1363.
- Isaev, S. A., P. A. Baranov, N. I. Vatin, Y. V. Zhukova and A. G. Sudakov (2014). Suppression of the Karman Vortex Street and Reduction in the Frontal Drag of a Circular Cylinder with Two Vortex Cells. *Technical Physics Letters* 40(8), 653-656.
- Janardhanan, S. and P. Thaliyakkattil (2015). Numerical Study on Aerofoil Stall. *International Conference on Emerging Research in Engineering Science and Technology*, Coimbatore, India.
- Katz, J. and A. Polotkin (1991). *Low-Speed Aerodynamics*. McGraw-Hill Series in Aeronautical and Aerospace Engineering, New York, 632.
- Kruppa, E. W. (1977). Wind Tunnel Investigation of the Kasper Vortex Concept. *13th annual meeting and technical display incorporating the forum on the future of air transportation*, Washington, DC, (Jan.), 10–13.
- Moran, J. (1984). *Theoretical and Computational Aerodynamics*. John Wiley and Sons, New York, 464.
- Narayana, P. A. A., K. A. Rasya and S. S. Prasad (2018). Effect of Outward and Inward Dimple Located on Different Positions of Aerofoil Section at a Typical Low Reynolds Number. *International Journal of Engineering and Technology* 7 (4.25), 29-34.
- Prasath, M. S. and S. I. Angelin (2017). Effect of Dimples on Aircraft Wing. *GRD Journals-Global Research and Development Journal for Engineering* 2(5), 234–242.
- Roy, J. F. (1988). *Fluides parfaits incompressibles*. Edition Marketing, Ellipses, France.
- Savitsky, A. I., L. N. Schukin, V. G. Karelin, R. M. Pushkin, A. M. Mass, A. P. Shibanov, I. L. Schukin and S. V. Fischenko (1995). Method for control of the boundary layer on the aerodynamic surface of an aircraft, and the aircraft provided with the boundary layer control system. *United States Patent*, 5417391.
- Sheldahl, R. E. and P. C. Klimas (1981). Aerodynamic Characteristics of Seven Symmetrical Airfoil Sections through 180-Degree Angle of Attack for Use in Aerodynamic Analysis of Vertical Axis Wind Turbines. *Sandia Natl. Labs., Albuquerque, NM* 80-2114, 19.
- Sørensen, N. (2009). Airfoil Computations Using the γ -Re θ Model. *Danmarks Tekniske Universitet, Risø Nationallaboratoriet for Bæredygtig Energi. Denmark. Forskningscenter Risoe. Risoe-R*, 1693(EN).
- Sowmyashree, Y., D. I. P. Aishwarya, S. Spurthy, R. Sah, B. V. Pratik, H. V. Srikanth and R. Suthan (2020). Study on Effect of Semi-Circular Dimple on Aerodynamic Characteristics of NACA 2412 Airfoil. *AIP Conference Proceedings* 2204(Jan.), 030009.
- Srivastav, D. (2012). Flow Control over Airfoils Using Different Shaped Dimples. *IPCSIT* 33, 92-97.
- Tang, L. (2008). Reynolds-averaged Navier-Stokes simulation of low-Reynolds-number airfoil aerodynamics. *Journal of Aircraft* 45(3), 848-856